

# X-ray detection based on complementary metal-oxide-semiconductor sensors

Qian-Qian Cheng<sup>1</sup> · Chun-Wang Ma<sup>1</sup> · Yan-Zhong Yuan<sup>2</sup> · Fang Wang<sup>2</sup> · Fu Jin<sup>3</sup> · Xian-Feng Liu<sup>3</sup>

Received: 7 August 2018 / Revised: 23 October 2018 / Accepted: 3 November 2018 / Published online: 2 January 2019  
© China Science Publishing & Media Ltd. (Science Press), Shanghai Institute of Applied Physics, the Chinese Academy of Sciences, Chinese Nuclear Society and Springer Nature Singapore Pte Ltd. 2019

**Abstract** Complementary metal-oxide-semiconductor (CMOS) sensors can convert X-rays into detectable signals; therefore, they are powerful tools in X-ray detection applications. Herein, we explore the physics behind X-ray detection performed using CMOS sensors. X-ray measurements were obtained using a simulated positioner based on a CMOS sensor, while the X-ray energy was modified by changing the voltage, current, and radiation time. A monitoring control unit collected video data of the detected X-rays. The video images were framed and filtered to detect the effective pixel points (radiation spots). The histograms of the images prove there is a linear relationship between the pixel points and X-ray energy. The relationships between the image pixel points, voltage, and current were quantified, and the resultant correlations were observed to obey some physical laws.

**Keywords** X-ray detection · Simulated positioner · Complementary metal-oxide-semiconductor sensor · Effective pixel points

---

This work was supported by the Plan for Science Innovation Talent of Henan Province (No. 154100510007), the Natural and Science Foundation in Henan Province (No. 162300410179) and the Cultivation Foundation of Henan Normal University National Project (No. 2017PL04).

---

✉ Chun-Wang Ma  
machunwang@126.com

<sup>1</sup> College of Physics and Materials Science, Henan Normal University, Xinxiang 453007, China

<sup>2</sup> College of Electronic and Electrical Engineering, Henan Normal University, Xinxiang 453007, China

<sup>3</sup> Chongqing Cancer Hospital, Chongqing 400030, China

## 1 Introduction

Complementary metal-oxide-semiconductor (CMOS) sensors have several applications, owing to their ability to convert X-rays and  $\gamma$ -rays into a bright spot on the image [1, 2]. Apart from Chandra, concepts for future large X-ray astrophysics missions have already been well developed [3]. In addition, the technical aspects of CMOS X-ray detectors have been developed significantly. By focusing on space-based X-ray observatories, the Penn State X-ray detector lab has developed new small pixel hybrid CMOS X-ray detectors [4]. In medicine, high-performance X-ray detectors based on CMOS active pixel sensors have been developed and proposed for digital breast tomosynthesis [5–7].

CMOS sensors can be employed to detect low energy X-rays or  $\gamma$ -rays for imaging [8, 9] or dosimetry [10–14]. Diagnostic X-ray dosimetry uses the current or charge obtained using an ionizing radiation sensor, which is amplified using a special weak signal amplifier and collected with the data collector and microprocessor, combined with different mathematical models to correct the radiation energy value [15]. A smartphone application (app) using the built-in camera equipped with a CMOS sensor was designed by Wei et al. [16] to survey the ionization radiation of the environment.

Thus, a CMOS sensor can be used to detect X-rays. In this study, we explore the physical laws behind this phenomenon.

## 2 Materials and methods

### 2.1 Experimental setup

The schematic diagram of the system is shown in Fig. 1. X-ray photons are generated using the Acuity™ Simulator, produced by American Varian. The Acuity™ Simulator can fix the position of the tumor region in a radiotherapy patient and simulate the accelerator parameter. When the voltage and current change with the radiation time, the energy of the X-ray photons is adjusted. A monitoring control unit produced by Shenzhen Stjiatu Technology Co., Ltd (STJIATU) is used. It comprises a CMOS image sensor, video recorder, and liquid-crystal display (LCD). The CMOS image sensor was adopted as the key part of the X-ray detector to receive X-rays without any scintillator [17]. The pixel architecture of the CMOS sensor is based on silicon photodiode active pixel sensor technology. When an X-ray photon impinges on the CMOS sensor, a current is generated on the PN junction of the photodiode [18]. In this case, a bright spot appears on the image [17]. Owing to the Compton effect, the energy loss is insignificant [19]. The bright image is displayed on the LCD display and saved as a video using a video recorder.

The camera was covered by a film to reduce the influence of the infrared light produced by the lamps. Figure 2 shows the schematic of the X-ray detection experiment, which was conducted without visible light.

### 2.2 Data analysis methods

The analyzed image was in grayscale, where the gray region indicates the image brightness or color shading [14]. The gray value method has been adopted in various image processing applications for satellite images, aerial photographs, and geophysical observations [20]. The color values of a certain pixel in the original image (red, green, and blue) were transformed into grayscale values according to the following equation [21]:

$$G = (30 \times \text{Red} + 59 \times \text{Green} + 11 \times \text{Blue})/100. \quad (1)$$

The background threshold is obtained by analyzing the rule of pixel maximum rendered by radiation-free pictures: The pixel value of a valid data picture with radiant highlights is greater than the background threshold.

First, the video data obtained from the experiment were divided into images by using MATLAB. Subsequently, images with valid data were filtered from these pictures

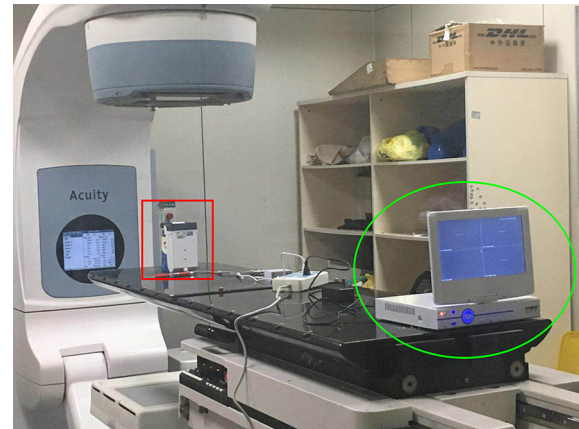


**Fig. 2** (Color online) Schematic of the X-ray detection experiment. The red rectangle indicates the CMOS camera, and the green circle indicates the recorder and LCD display

using the background threshold. Simultaneously, the background threshold was used to filter out the background noise. If a pixel point has a value lower than the background threshold, it is considered to be zero; otherwise, it is regarded as an effective pixel point. A filtered grayscale image without background noise is shown in Fig. 3.

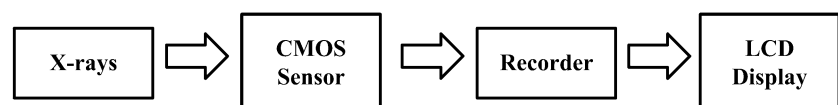
Image histograms are used to illustrate the relationship between the gray levels and their frequencies. If the total number of pixels in an image is  $N$ , the number of gray levels is  $L$ , and the total number of pixels in the  $k$ th gray level with gray  $r_k$  is  $n$ , the probability that the  $k$ th gray level appears can be expressed as follows:

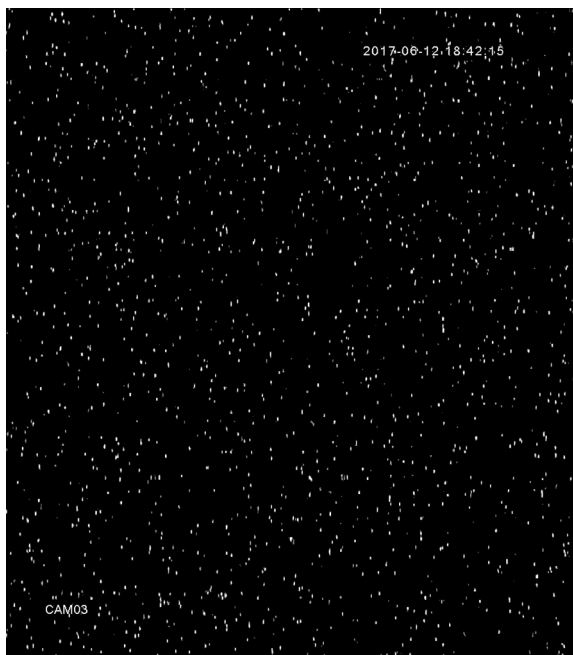
$$p(k) = n_k/N \quad (k = 0, 1, \dots, L - 1). \quad (2)$$

Figure 4 shows the image histograms for a group of images with 80 mA and 250 ms. The voltages in Fig. 4a, b correspond to 115 kV and 60 kV, respectively. In Fig. 4, when the gray level is 255, the corresponding  $p$  is highest, which indicates that there are many white pixel points. Figure 4 shows that there is a certain relationship between the gray value and voltage. In Fig. 4a, for centrally distributed effective pixels, when the voltage is 115 kV, the gray distribution is higher and more focused in comparison with that in Fig. 4b.

Considering that the effective pixel points correspond to the radiation energy, we use the number of effective pixel points and the sum of their gray values to quantify the relationship between the gray value and voltage. As we collected videos using various voltages and currents at different points in time, the number of images in each

**Fig. 1** Schematic diagram of the system





**Fig. 3** Grayscale image without background noise (80 mA; 250 ms; 60 kV)

group is different. Therefore, we normalized the aforementioned two physical quantities.

### 3 Results

To investigate the correlation between the two physical quantities and radiation energy, we perform linear fitting on the obtained values, as shown in Figs. 5, 6, 7 and Tables 1, 2, 3.

**Fig. 4** (Color online) Grayscale image histogram without background noise (80 mA; 250 ms)

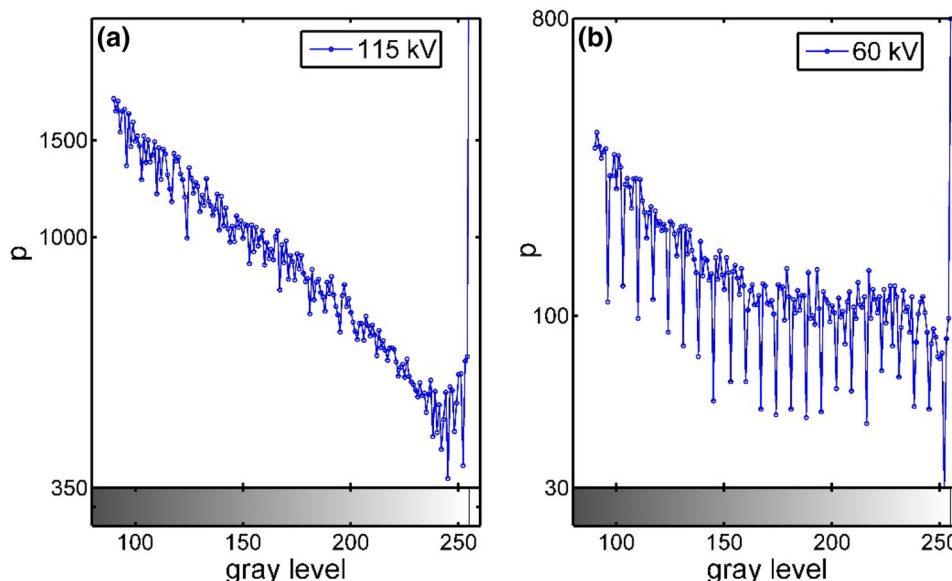


Figure 5a shows the correlation between the voltage and the number of effective pixel points when the current is 25, 50, and 80 mA. There are three distribution trends that reflect the correlation between the gray value and voltage at three different current values. The specific differences in the fitting results are summarized in Table 1. The  $R^2$  values of the sum of the gray values of all the effective pixels are lower than those of the number of effective pixel points.

The correlations between the electron current and the number of effective pixel points for the voltages of 60, 95, and 125 kV are shown in Fig. 6a. Figure 6b presents the correlation between the electron current and the sum of the gray values of all the effective pixel points.

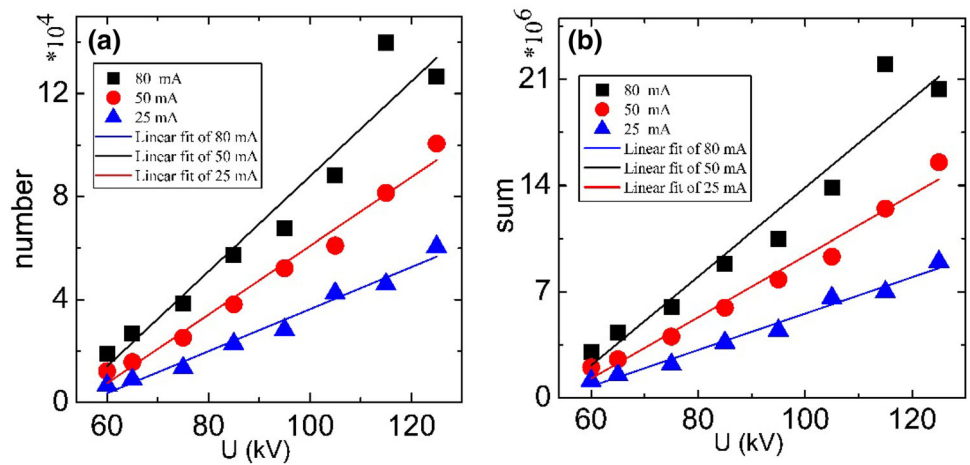
The three observed distribution trends for the two physical quantities are similar; specific differences in the fitting results are summarized in Table 2. The  $R^2$  values of the sum of the gray values of all the effective pixels are lower than those of the number of effective pixel points.

Figure 7 shows the correlation between the voltage and the two physical quantities with the corresponding linear function fitting at different times. The distribution trends of the number of effective pixel points and the sum of their gray values are similar; specific differences in the fitting results are summarized in Table 3. The influence of time on the radiation energy of the X-rays is considerably small.

### 4 Conclusion

An experiment for X-ray detection based on CMOS sensors was designed. In this experiment, various voltages and currents were used to control the energy of X-rays. Furthermore, video data were collected using a detector at

**Fig. 5** (Color online) Correlation between the voltage and the two physical quantities with the corresponding linear function fitting based on the different current values. Number and sum, respectively, indicate the number of effective pixel points and the sum of their gray values



**Fig. 6** (Color online) Correlation between the current and the two physical quantities with the corresponding linear function fitting for three different voltage values.  $I$  denotes the electron current

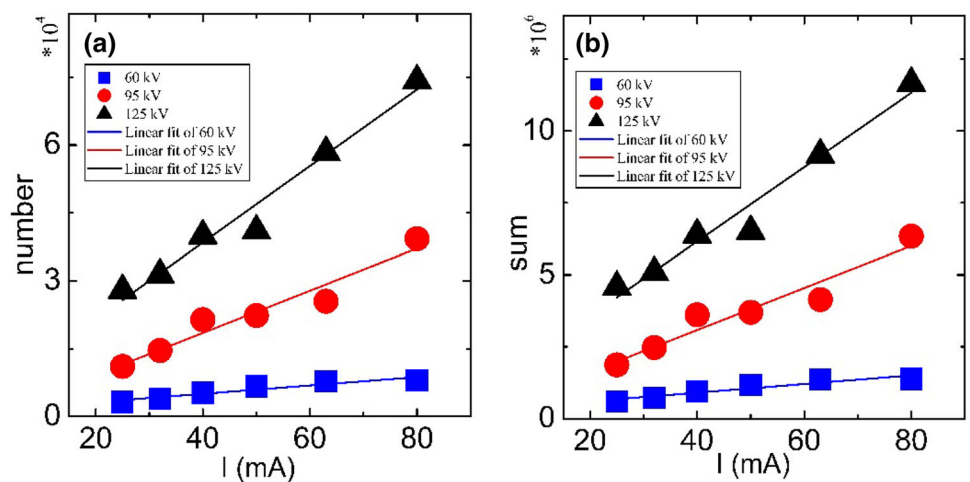
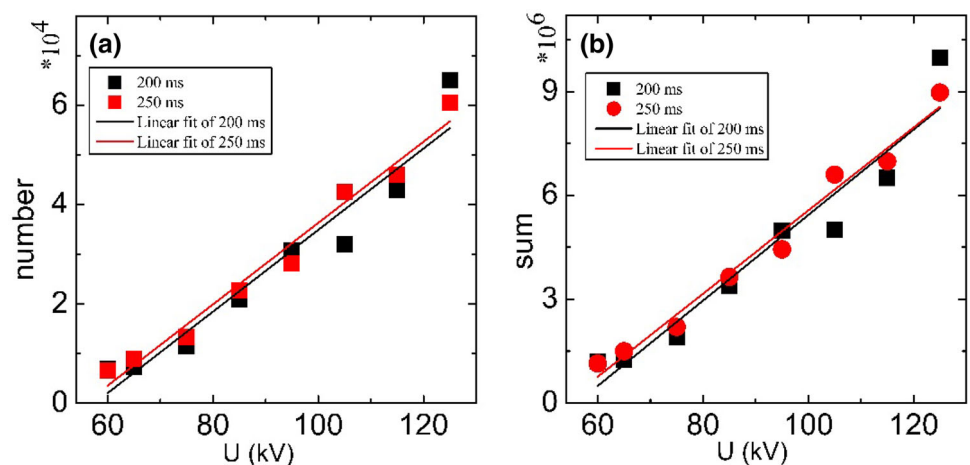


**Fig. 7** (Color online) Correlation between the voltage and the two physical quantities with the corresponding linear function fitting at different times



different points in time and images of valid data were obtained from the video data via framing and screening based on a background threshold. As shown in the image histograms, the relationship between the effective pixel

points and radiation energy was quantified. With an increase in the voltage and current, we obtained more effective pixel points, and the gray distribution in the image histograms was higher and more intensive. To determine the correlation

**Table 1** Comparison of the fitting results between the number of effective pixel points and the sum of their gray values for three current values

Equation	$y = a + b \times x$	Number	Sum
25 mA	$R^2$	0.97387	0.97782
	Intercept	- 4.5513	- 6.4407
	Slope	0.0818	0.12005
50 mA	$R^2$	0.97921	0.97505
	Intercept	- 7.2536	- 10.841
	Slope	0.13336	0.20198
80 mA	$R^2$	0.92582	0.92692
	Intercept	- 9.6608	- 15.422
	Slope	0.18446	0.29279

**Table 2** Comparison of the fitting results between the number of effective pixel points and the sum of their gray values for three different voltage values

Equation	$y = a + b \times x$	Number	Sum
60 kV	$R^2$	0.88215	0.87442
	Intercept	0.1315	0.29771
	Slope	0.0092	0.01513
95 kV	$R^2$	0.92779	0.91666
	Intercept	- 0.0172	0.15996
	Slope	0.0466	0.07306
125 kV	$R^2$	0.96311	0.95958
	Intercept	0.4582	0.9877
	Slope	0.0846	0.12931

**Table 3** Comparison of fitting results between the number of effective pixel points and the sum of their gray values

Equation	$y = a + b \times x$	Number	Sum
200 ms	$R^2$	0.9185	0.9159
	Intercept	- 4.71	- 6.906
	Slope	0.082	0.1233
250 ms	$R^2$	0.973	0.9778
	Intercept	- 4.55	- 6.440
	Slope	0.081	0.1200

between the effective pixel points, voltage, and current, we fitted the experimental data of the two physical quantities—the number of effective pixel points and the sum of their gray values—with a linear function. The fitting results showed that both measurements linearly changed with the voltage and current but were not affected by time.

**Acknowledgements** We thank Dr. Gong-Tao Fan and Prof. Hong-Wei Wang of Shanghai Institute of Applied Physics, CAS, for their kind help in the experiments.

## References

- M.J. Yaffe, J.A. Rowlands, X-ray detectors for digital radiography. *Phys. Med. Biol.* **42**, 1 (1997). <https://doi.org/10.1088/0031-9155/42/1/001>
- X. Wang, S.L. Zhang, G.X. Song et al., Remote measurement of low-energy radiation based on ARM board and ZigBee wireless communication. *Nucl. Sci. Tech.* **29**, 4 (2018). <https://doi.org/10.1007/s41365-017-0344-2>
- X. Wang, P. Knapp, S. Vaynman et al., Experimental study and analytical model of deformation of magnetostrictive films as applied to mirrors for X-ray space telescopes. *Appl. Opt.* **53**(27), 6256–6267 (2014). <https://doi.org/10.1364/AO.53.006256>
- Z. Prieskorn, C.V. Griffith, S.D. Bongiorno et al., Characterization of Si hybrid CMOS detectors for use in the soft X-ray band. *Nucl. Instrum. Methods Phys. A* **717**, 83–93 (2013). <https://doi.org/10.1016/j.nima.2013.03.057>
- C. Zhao, N. Vassiljev, A.C. Konstantinidis et al., Three-dimensional cascaded system analysis of a 50  $\mu\text{m}$  pixel pitch wafer-scale CMOS active pixel sensor X-ray detector for digital breast tomosynthesis. *Phys. Med. Biol.* **62**, 1994 (2017). <https://doi.org/10.1088/1361-6560/aa586c>
- T. Patel, H. Peppard, M.B. Williams, Effects on image quality of a 2D anticatter grid in X-ray digital breast tomosynthesis: initial experience using the dual modality (X-ray and molecular) breast tomosynthesis scanner. *Med. Phys.* **43**, 1720–1735 (2016). <https://doi.org/10.1118/1.4943632>
- D. Magalotti, P. Placidi, M. Dionigi et al., Experimental characterization of a personal wireless sensor network for the medical X-ray dosimetry. *IEEE Trans. Instrum. Meas.* **65**, 2002–2011 (2016). <https://doi.org/10.1109/TIM.2016.2534661>
- D.W. Lane, X-ray imaging and spectroscopy using low cost COTS CMOS sensors. *Nucl. Instrum. Methods Phys. B* **284**, 29–32 (2012). <https://doi.org/10.1016/j.nimb.2011.09.007>
- S.L. Zhang, Q.Q. Cheng, D.F. Guo et al., Design of the new remote measurement system for low-energy radiation. *Nucl. Electron. Detect. Technol.* **37**, 262–267 (2017). <https://doi.org/10.3969/j.issn.0258-0934.2017.03.008>
- Q.Q. Cheng, Y.Y. Zhong, C.W. Ma et al., Gamma measurement based on CMOS sensor and ARM microcontroller. *Nucl. Sci. Tech.* **28**, 122 (2017). <https://doi.org/10.1007/s41365-017-0276-x>
- D. Magalotti, L. Bissi, E. Conti et al., Performance of CMOS imager as sensing element for a real-time active pixel dosimeter for interventional radiology procedures. *J. Instrum.* **9**, C01036 (2014). <https://doi.org/10.1088/1748-0221/9/01/C01036>
- E. Conti, P. Placidi, M. Biasini et al., Use of a CMOS image sensor for an active personal dosimeter in interventional radiology. *IEEE Trans. Instrum. Meas.* **62**, 1065–1072 (2013). <https://doi.org/10.1109/TIM.2012.2223331>
- M. Pérez, J. Lipovetzky, M.S. Haro et al., Particle detection and classification using commercial off the shelf CMOS image sensors. *Nucl. Instrum. Methods Phys. A* **827**, 171–180 (2016). <https://doi.org/10.1016/j.nima.2016.04.072>
- F. Wang, M.Y. Wang, Y.F. Liu et al., Obtaining low energy  $\gamma$  dose with CMOS sensors. *Nucl. Sci. Tech.* **25**, 060401 (2014). <https://doi.org/10.13538/j.1001-8042/nst.25.060401>
- T. Ishiwatari, G. Beer, A.M. Bragadireanu et al., New analysis method for CCD X-ray data. *Nucl. Instrum. Methods Phys. A* **556**, 509–515 (2006). <https://doi.org/10.1016/j.nima.2005.10.105>
- Q.Y. Wei, R. Bai, Z.P. Wang et al., Surveying ionizing radiations in real time using a smartphone. *Nucl. Sci. Tech.* **28**, 70 (2017). <https://doi.org/10.1007/s41365-017-0215-x>
- F. Wang, M.Y. Wang, F.S. Tian et al., Study on two-dimensional distribution of X-ray image based on improved Elman algorithm.

- Radiat. Meas. **77**, 1–4 (2015). <https://doi.org/10.1016/j.radmeas.2015.03.012>
18. A.C. Konstantinidis, M.B. Szafraniec, R.D. Speller et al., The Dexela 2923 CMOS X-ray detector: a flat panel detector based on CMOS active pixel sensors for medical imaging applications. Nucl. Instrum. Methods Phys. A **689**, 12–21 (2012). <https://doi.org/10.1016/j.nima.2012.06.024>
  19. H.G. Kang, J.J. Song, K. Lee et al., An investigation of medical radiation detection using CMOS image sensors in smartphones. Nucl. Instrum. Methods Phys. A **823**, 126–134 (2016). <https://doi.org/10.1016/j.nima.2016.04.007>
  20. W. Kang, H. Li, F. Deng, Direct gray-scale extraction of topographic features for vein recognition. Sci. China Inf. Sci. **53**, 2062–2074 (2010). <https://doi.org/10.1007/s11432-010-4064-z>
  21. J.C. Russ, *The Image Processing Handbook* (CRC Press, Boca Raton, 2016)